Arabian Journal of Geosciences (2020) 13: 977
https://doi.org/10.1007/s12517-020-05867-w

ORIGINAL PAPER

Characteristics and implication of multilayer dawsonite in heterogeneity reservoir of the Honggang anticline, southern Songliao Basin, NE China

Na Liu[1] · Li Liu[1] · Xiaoran Ming[2] · Lei Yu[1]

Received: 12 June 2020 / Accepted: 13 August 2020 / Published online: 17 September 2020

Abstract
Reservoir heterogeneity is one of the key factors regarding the long-term fate of the injected CO_2. Natural CO_2 reservoir and ancient CO_2-bearing reservoir is a natural analog to investigate the influence of reservoir heterogeneity on the migration of CO_2 and CO_2-rock interaction with geological timescale. Dawsonite cements are detected in both sandstone and mudstone of the Upper Cretaceous Qingshankou reservoir in Honggang anticline of the southern Songliao Basin, China. Here, we present results of a petrographic characterization of this reservoir based on polarizing microscope, X-ray diffraction, and fluid inclusion data. These data were used to identify the vertical distribution characteristic of dawsonite and to identify the migration characteristics for the supercritical CO_2 in heterogeneity reservoir. Our analytical results show that as the "CO_2 trace mineral," dawsonite appears as multilayered zones of cementation that are separated by mudstone interlayers. These multilayered dawsonite could be one of the geological produces for supercritical CO_2 flooding through the heterogeneous rock, acting as the lateral migration and upward diffusion. Supercritical CO_2 could move through the thinner mudstone interlayer, with the product of dawsonite developing in the mudstone as its "footprint," although the vertical distance of diffusion in low-permeability caprock is limited. Combined with the truth that most of the present CO_2 gas reservoirs (in K1q4) are in the deeper layers than the dawsonite-bearing sandstone (K1q4-K2y1) (developed in non-CO_2 reservoir), we can deduce that CO_2 was at some time abundant in the Honggang anticline but had now part of CO_2 been migrated, with the other part consumed by the reaction with the primary rock and captured as new carbonate minerals. The dawsonite-bearing sandstones also record a sequence of hydrocarbon filling events. Combined with the truth that the injection time of CO_2 is later than that of hydrocarbon, the early hydrocarbon should be deasphalted by the injection and migration of mantle CO_2. Therefore, CO_2 could also be stored as long-term carbonate minerals after the termination of a CO_2-EOR project.

Keywords Dawsonite · Multilayer distribution · Supercritical CO_2 · CO_2 migration · Songliao Basin

Introduction

Monitoring and determination of the underground CO_2 plume migration is one of the great challenges in carbon capture and storage (CCS) development (IPCC 2005; Aminu et al. 2017; Shin and Son 2018; Karimi et al. 2018; Giuliano et al. 2019). Reservoir heterogeneity at various length scales is a well-established fact, and the heterogeneity is a key factor influencing the long-term security of CO_2 geological storage. The long-term fate for the injection CO_2 in CCS has been predicted by numerical simulations, while the traditional homogeneous geological models are likely to be too simple given the strong heterogeneity of the reservoirs in the case of CO_2 injection. Nowadays, a series of laboratory experimental (Park et al. 2017) and geological numerical simulations (Al-Khdheeawi et al. 2018; Qiao et al. 2020) focus on characterizing CO_2 plume migration in multilayer reservoirs with strong heterogeneity. In fact, natural CO_2-bearing reservoirs can also provide a natural analog for CO_2 migration in heterogeneity reservoir.

This article is part of the Topical Collection on *Big Data and Intelligent Computing Techniques in Geosciences*

✉ Li Liu
liuli0892@vip.sina.com

[1] College of Earth Sciences, Jilin University, Changchun 130061, China

[2] The First Monitoring and Application Center, China Earthquake Administration, Tianjin 300180, China

Dawsonite has been identified as a possible carbonate product resulting from the injection of CO_2 into the sandstone reservoirs, such as in the Permian Supai Formation of Springerville Field, USA (Moore et al. 2005); the BGS basin system, Eastern Australia (Baker et al. 1995; Golab et al. 2006); the Lam Formation of Shabwa Basin, Yemen (Worden 2006); the Nantun Formation of Hailar Basin, China (Gao et al. 2009); the Qingshankou Formation of south Songliao Basin, China (Liu et al. 2011; Yu et al. 2014); and the Mingyuefeng Formation of Lishui Sag, China (Zhao et al. 2018). Numerical simulations (Zhang et al. 2004; Álvarez-Ayuso and Nugteren 2005; Hellevang et al. 2005, Okuyama et al. 2009; Shi et al. 2019) and thermodynamic calculations imply that dawsonite grows under elevated CO_2 pressure conditions (partial pressures of CO_2 is at least 50 bar) or when abundant CO_3^{2-} or HCO_3^- is coupled with aluminosilicate dissolution. However, a debate exists concerning the status of dawsonite and the possibility of precipitating this phase in an artificial CO_2 storage in sandstones. Some researchers hold that dawsonite will become unstable as CO_2 pressure decreases following injection through equilibrium-based experimental and modeling evaluation (Hellevang et al. 2005, 2014; Bénézeth et al. 2007; Kaszuba et al. 2011; Kampman et al. 2014). They argue that the lack of nucleation and growth rate data for dawsonite, the lack of dawsonite growth in laboratory experiment under CO_2 storage conditions, and the uncertainty in growth conditions for the natural analogues rendered numerical predictions highly uncertain. In any case, precipitation of dawsonite induced by CO_2 injection is supported by field observations (e.g. Baker et al. 1995; Moore et al. 2005; Noh et al. 2018; Worden 2006; Zhao et al. 2018). In Permo-Triassic sedimentary rocks of the Bowen-Gunnedah-Sydney basin system, eastern Australia, dawsonite is widespread as a cement, replacement, and cavity filling, while the distribution and interpreted origin of dawsonite (magmatic carbon source) imply that magmatic CO_2 seepage into the Permo-Triassic sequences on a continental scale (Baker et al. 1995).

The Honggang anticline, which is located in the southern Songliao Basin, NE China, is an ideal area for studying the indicators of CO_2 migration on account of the development of abundant dawsonite cements (Liu et al. 2011) and the presence of a locally developed CO_2-bearing gas reservoir within the anticline (Hou et al. 2009). The sandstone reservoir of the Honggang anticline contains oil, gas, and mantle-magmatic CO_2. The injection of oil-gas is demonstrated by the existence of oil-gas-bearing inclusions and the intergranular oil staining in the sandstones, while the injection of CO_2 is recorded by the presence of carbonate minerals that formed during CO_2-rock interaction, such as dawsonite (Liu et al. 2011).

Several petrographic studies have been undertaken on the Quantou and Qingshankou Formation in the Honggang area, many of which were contracted by oil companies to assess reservoir quality (Niu et al. 2012). Recent studies of the Honggang area have investigated the interaction of CO_2 with the minerals in sandstones (Liu et al. 2011) and mudstones (Wang 2013; Ming 2017). The mineralogy, diagenetic features, and isotopic compositions of dawsonite-bearing sandstones in the Honggang anticline have been characterized by Liu et al. (2011), who found that the mineral assemblage that formed after CO_2 flooding comprises dawsonite, microcrystalline quartz II, kaolinite II, calcite II, and ankerite. Some dawsonite cements have been detected in mudstones using X-ray diffraction (Ming 2017). These aforementioned studies have described the diagenetic effects caused by CO_2 injection within a single reservoir interval over geological time.

For the present study, we focus on the Lower Cretaceous Qingshankou Formation, which is producing hydrocarbon reservoir, and aim to discuss the spatial distribution characteristic of dawsonites within dawsonite-bearing sandstones and dawsonite-bearing mudstones of the Honggang anticline. The results of the study contribute to understanding the CO_2 migration characteristics in the heterogeneity reservoir with geological timescale.

Geological background

The Songliao Basin is the largest Mesozoic-Cenozoic sedimentary basin in the Cathaysian system and the largest oil-producing province in China (Xu et al. 2000). The Qingshankou and Nenjiang mudstones were deposited during two large lake-flooding events in the Songliao Basin and constituted the main hydrocarbon source rocks and major reservoirs in the basin (Zhang and Bao 2009). The Honggang anticline is one of the subordinate structural belts of the central depression in Songliao Basin (Fig. 1). From the end of deposition of the Nenjiang Formation to the end of deposition of the Mingshui Formation, the whole of the Honggang area was occupied by an anticline with the axis trending NS (Chen, 2003). There are mainly three stages of structure evolution in Songliao Basin, including rift stage, depression stage, and inversion stage. Strong fault activities went through these three stages. Honggang fault, as the basement fault, is cutting through the T5 reflection layer, upward through the T02 reflection layer (Fig. 1). This fault was active from Carboniferous and Permian, but the most active period of it was during late K1q-early K2qn and structural inversion stage (Fig. 3) (Liu et al. 2018).

The burial history in this area during the Late Cretaceous included a punctuated rifting stage into a maximum burial (~ 2400 m) and maximum temperature (~ 117 °C) in Paleocene, a modest uplift stage, leading to a reduction in the ambient temperature of the sedimentary rocks (Fig. 2) (Zou et al. 2005; Yang et al. 2010). The average geothermal gradient and heat flow in the Paleocene was about 4.26 °C/m and 95–107 mW/

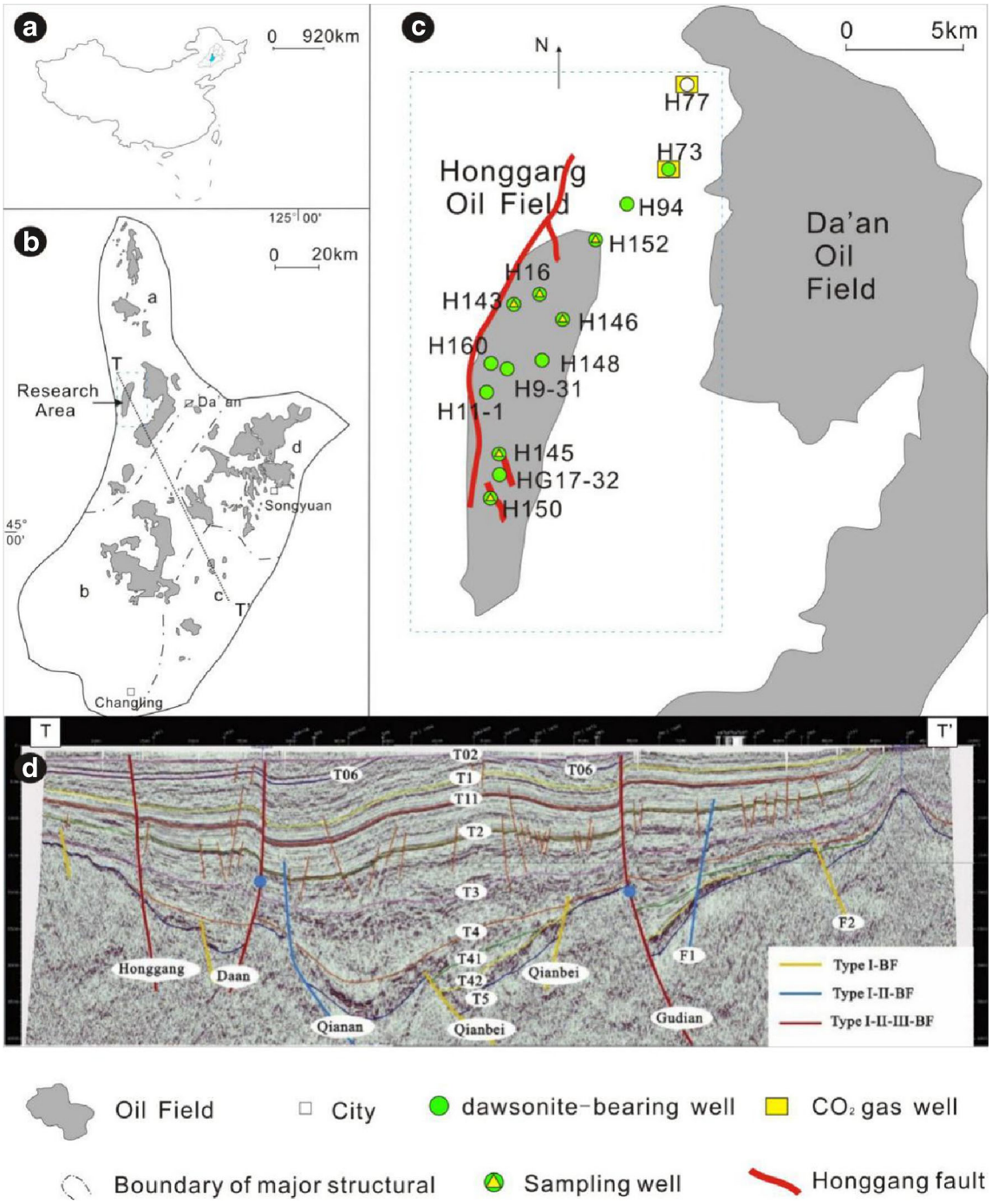

Fig. 1 Map of the S corner of the Songliao Basin showing the research area in Honggang. The locations of the wells containing dawsonite-bearing sandstones are marked. (A) Location of Songliao Basin; (B) boundary of major structural units for southern part of Songliao Basin: (a) Honggang Step, (b) Changling Depression, (c) Huazijing Step, and (d) Fuxin Uplift; (C) researching area and distribution of dawsonite-bearing sandstones containing well; (D) cross section for southern part of Songliao Basin according to Liu et al. (2018); I-BF: the basement faults being continuously active during the syn-rift stage only cutting through the T4 or T5 reflection layer; I-II-BF: the basement faults being continuously active during the period from the syn-rift to post-rift stages cutting through the T4 or T5 reflection layer, upward through the T2 reflection layer; I-II-III-BF: the basement faults being continuously active during the period from the syn-rift stage to structural inversion stage cutting through the T4 or T5 reflection layer, upward through the T02 reflection layer

m^2, respectively (Ren et al. 2001). The present-day reservoirs' temperature and pressure are 73 ~ 99 °C and 12.5 ~ 18.7 Mpa (Ren et al. 2001).

Dawsonite-bearing sandstones are widespread in the Upper Cretaceous strata (Fig. 3). During the Late Cretaceous, as a regional transgression prevailed, many types of delta deposits

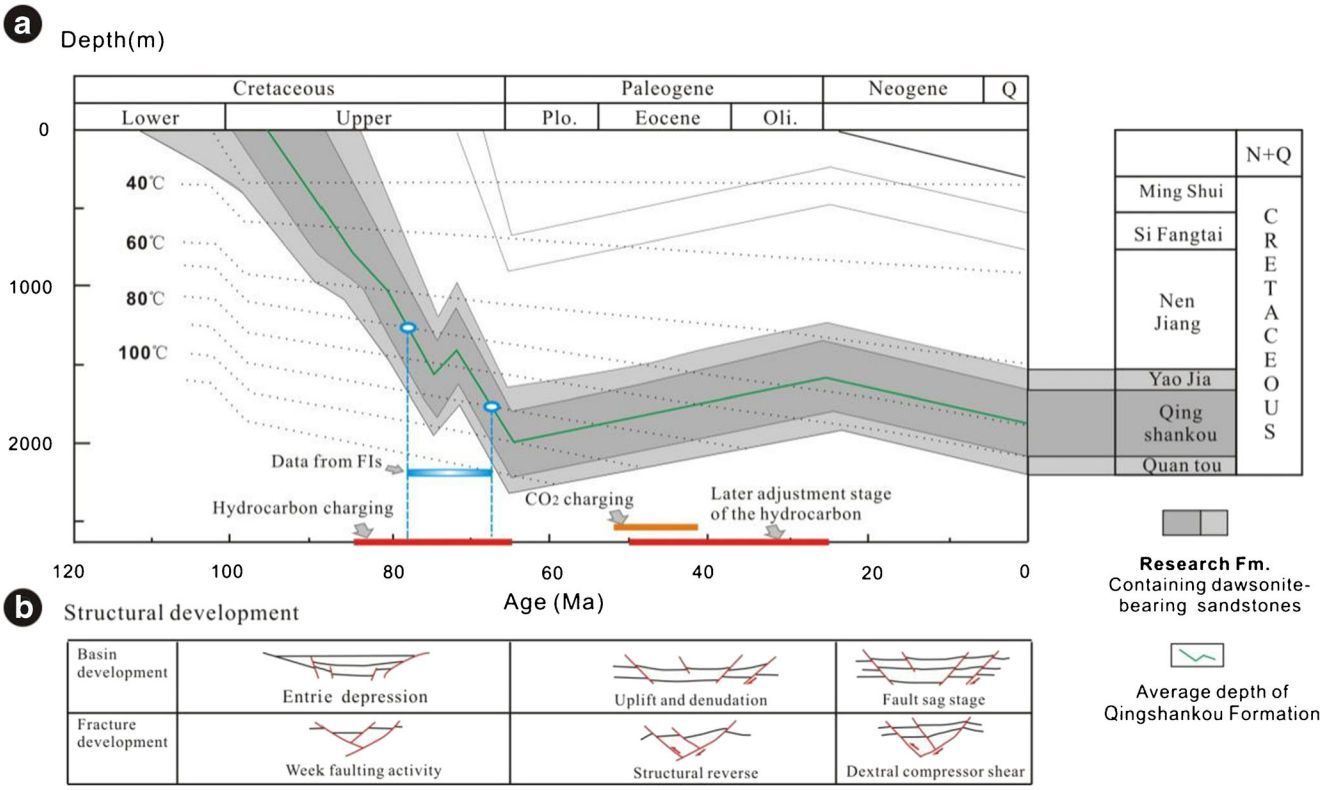

Fig. 2 (A) General burial-thermal history of H75# in Honggang anticline. The time of oil and CO_2 gas flooding are indicated (Zou et al. 2007; Yang et al. 2010). (B) Basin development and fracture development for the south of Songliao Basin according to Zou et al. (2007)

are formed, including those of the Qingshankou and Yaojia formations, Members 3 and 4 of the Nenjiang Formation, and Member 1 of the Mingshui Formation (Ge et al. 2012).

The oil in the reservoir was sourced from the Qingshankou mudstones (Wu et al. 2006; Zou et al. 2007). Recent studies on the timing of hydrocarbon accumulation carried out using conventional methods have shown that the accumulation of hydrocarbons in mid-depth strata of the southern Songliao Basin occurred mainly at Neijiang-Mingshui period (85–65 Ma) (Zou et al. 2005; Zou et al. 2007). However, there is an adjustment of the hydrocarbon at 50–25 Ma, due to the formation uplifting and erosion (Zou et al. 2007; Yu et al. 2014).

The CO_2-bearing gas reservoir (K1q3 + 4 and K2qn2 + 3 formation) is mainly located in the inverted structure belts that are controlled by the inversion of basement faults (Liu et al. 2018). Most of the researchers prefer a mantle-magmatic origin for the origin of CO_2 in the south of Songliao Basin according to the carbon and helium isotopic data ($\delta^{13}C_{CO2}$: −9.9 ~ −4.0 ‰, PDB; $^3He/^4He$: 2.65–5.88 × 10^{-6}, R/Ra: 1.9–4.56) (Dai et al. 1995; Chen et al. 1996; Lu et al. 2009; Fu et al. 2010; Qu et al. 2016). They hold that the volcanic eruption and the development of the related faults have a causal relationship with the formation of CO_2-bearing gas reservoirs.

In addition, geochemistry and geochronology of volcanic rocks in the study area indicate that the Shuangliao basalts were formed (41–51 Ma) during the structural inversion stage of Songliao Basin, and this basaltic magma is considered to have been the main source of CO_2 in the study area (Zhang 2006; Yu et al. 2014; Qu et al. 2016). In Honggang area, the presence of high content of inorganic CO_2 gas has been reported in K_1q^4 formation of wells H73# and H77#, which are located in the northeastern part of the field (Fig. 1). The values of pCO_2 for the wells H73# and H77# are 108 and 126 bar, with the content of CO_2 85 and 96%, respectively. The carbon isotope values of CO_2 ($\delta^{13}C_{CO2}$) range between − 8.05 and − 2.65‰ (PDB) (Yang et al. 2010). In Honggang, the formation waters for dawsonite-bearing reservoir appear as $NaHCO_3^-$-dominated waters, with a total salinity ranges of 8508.4 ~ 45,385 g/L, the concentrations of $K^+ + Na^+$, and HCO_3^- range of 2684.1 ~ 13,152.8 g/L and 3905.3 ~ 27,868.4 g/L, respectively.

Samples and methods

This study is based on the petrographic data from dawsonite-bearing sandstones in 14 wells (data of 351 thin sections, from Liu et al. 2011) and XRD data obtained from mudstones in 3

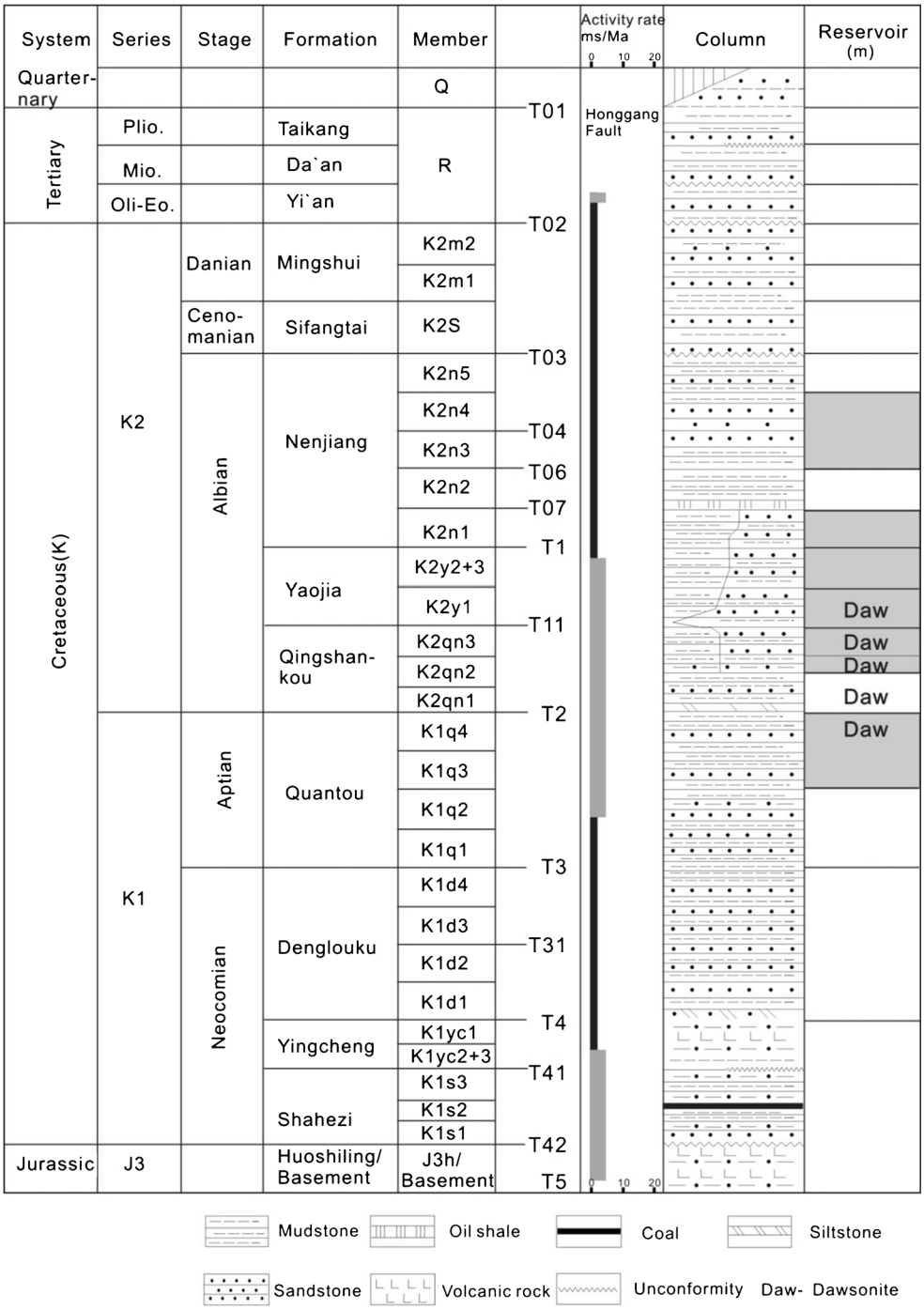

Fig. 3 Simplified stratigraphic chart for Songliao Basin. Dawsonite-bearing sandstones accumulated in the Quantou Formation, Qingshankou Formation, and Yaojia Formation. The activity rate for Honggang fault was according to Liu et al. (2018)

wells (37 sets of data, from Ming 2017). In addition, 30 core samples of the Qingshankou Formation and Yaojiao Formation were collected from 6 wells and prepared for thin-section examination. These 30 core samples were analyzed to obtain statistics on the contents of dawsonite and asphaltenes with line notation, which worked for 15 views. Combined with the well-logging data, these microscope-based content data were used to investigate the relationship between dawsonite content, asphaltene content, and the stratigraphic distributions of oil, gas, and formation water.

Observations of fluid inclusions in the dawsonite-bearing sandstones were conducted on four selected samples from H143# and H146# using a Leica DMRX HC fluorescence microscope in the Analytical Laboratory of Beijing Research Institute of Uranium Geology, Beijing, China. The fluid inclusion thermometry was performed using a LINKAM THMS600 heating-cooling stage with 1 °C precision.

Results

Petrographic characterization of the dawsonite-bearing sandstones

Dawsonite-bearing sandstones were found in drilling cuttings from 14 wells. Dawsonite is the most abundant cement in these sandstones, comprising 1–19% of the bulk rock volume. The identified dawsonite-bearing sandstones occur mainly in the Qingshankou Formation, with lower abundance in Member 4 of the Quantou Formation and in Member 1 of the Yaojia Formation (Fig. 4).

Samples of dawsonite-bearing sandstone from the Honggang anticline are poorly to moderately sorted lithic arkoses to feldspathic litharenites and contain 23–36% detrital quartz, 14–25% feldspar, and 16–35% rock fragments. Dawsonite is present as acicular crystal and radial aggregation filling pores or as bladed crystals and tufts/rosettes of fine needles replacing detrital grains or early-stage cements (Fig. 5a). Authigenic minerals in dawsonite-bearing sandstones (besides dawsonite) include quartz, feldspar, illite, kaolinite, illite-smectite, calcite, and ankerite. The order of cement growth can be summarized as feldspar overgrowth, quartz overgrowth, microcrystalline quartz I, kaolinite I, calcite I, dawsonite, microcrystalline quartz II, kaolinite II, calcite II, and ankerite (Liu et al. 2011).

Asphaltenes are abundant in dawsonite-bearing sandstone, comprising 0.7–7.2% of the whole rock by volume (Table. 1). This asphaltene is dark brown to gray brown, with a "bitumen-like" appearance on thin sections, and occurs in pores following feldspar dissolution (Fig. 5b), in small intergranular pores (Fig. 5c, e), and in intergranular pores of residual dawsonite aggregations (Fig. 5b). Some asphaltenes occur along cracks in minerals, constituting asphaltene veins (Fig. 5d), or as solid inclusions within ankerite cement (Fig. 5c). There is a moderate positive relationship between asphaltenes and dawsonite contents (Table. 1; Fig. 6).

According to well-logging data, around 20% of the sandstones containing dawsonite are developed in oil-bearing layers. It is worth noting that asphaltenes are found in all of the dawsonite-bearing sandstones, regardless of whether they are oil-bearing or dry units.

Petrographic characterization of the mudstones

The mineral composition of the mudstones mainly contains quartz, clay minerals (illite, illite and smectite mixing layer), plagioclase, feldspars, pyrite, dawsonite, ankerite, and sider-

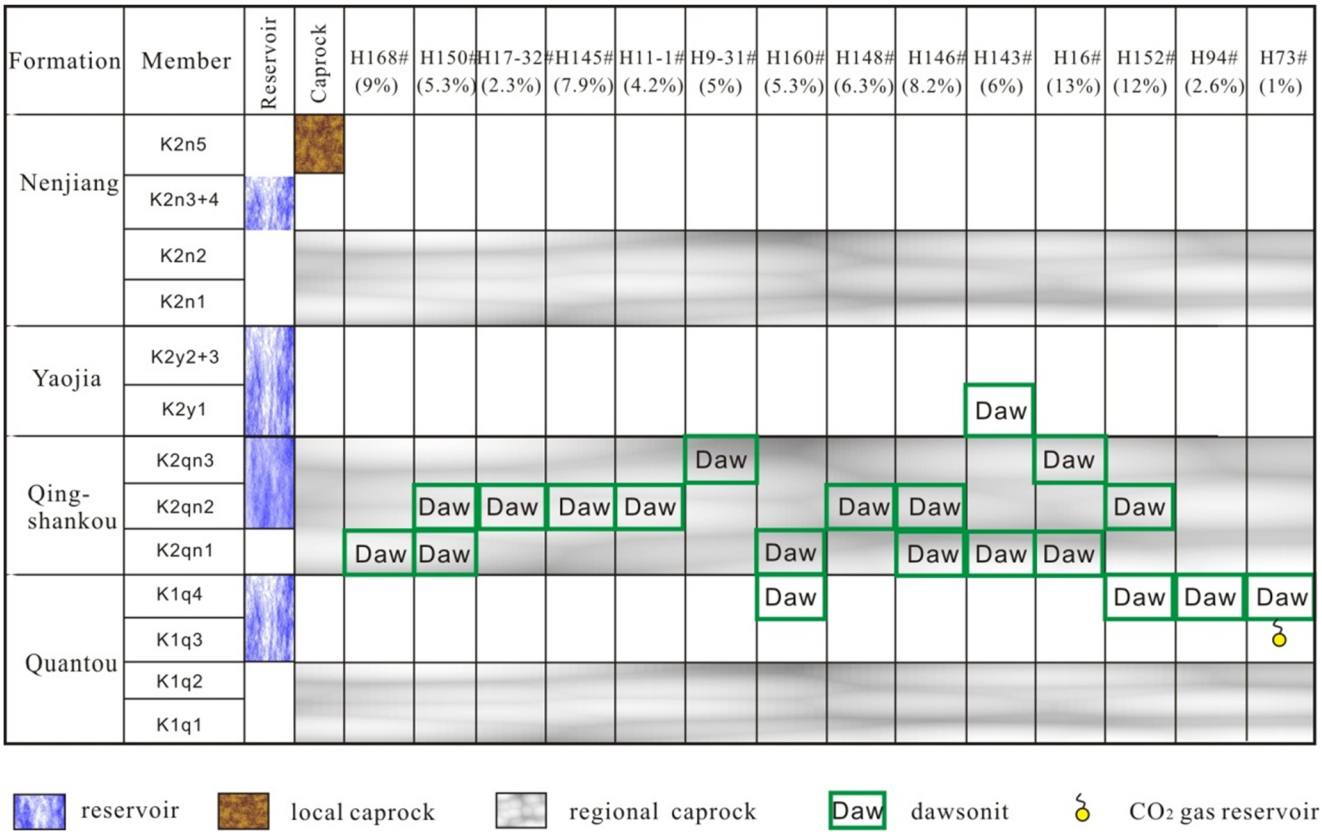

Fig. 4 Longitudinal distribution of dawsonite cements in Honggang anticline. Dawsonite-bearing sandstones accumulated in the Quantou Formation, Qingshankou Formation, and Yaojia Formation. The data in brackets is the average content of dawsonite in each well

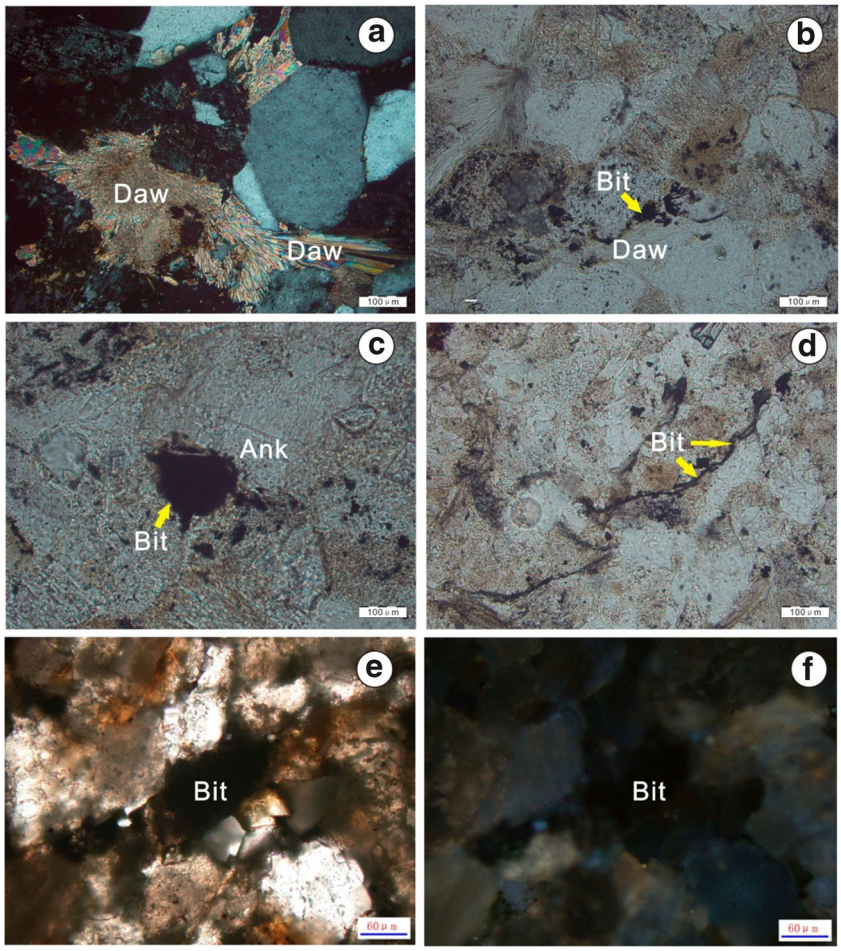

Fig. 5 Characteristic thin-section micrographs for dawsonite and asphaltenes in dawsonite-bearing sandstones. (a) Dawsonite filled in the porosity, present as acicular radial aggregations and bladed crystals, H146#, 1507.21 m, plane polarized light; (b) asphaltenes occur in pores following feldspar dissolution and the intergranular pores of residual dawsonite aggregations, H146#, 1507.21 m, plane polarized light; (c) disseminated asphaltenes, H146#, 1507.21 m, plane polarized light; (d) asphaltenes occur along cracks in minerals, constituting bitumen veins, H143#, 1256 m, plane polarized light; (e) asphaltenes occur in intergranular pores, H146#, 1550.41 m, plane polarized light; (f) asphaltenes occur in intergranular pores, the same site as (e), ultraviolet light. Daw, dawsonite; Bit, asphaltenes; Ank, ankerite

ite. The content of dawsonite in dawsonite-bearing mudstones ranges between 2 and 5.6% of the bulk rock volume with XRD analyzed (Table. 3). Dawsonite is difficult to recognize in mudstones as the dawsonite crystals are so small that visual detection is usually impossible.

Vertical distribution of dawsonite cements

In this study, we focused on the vertical distribution of dawsonite cement in the well of H145#, H146#, and H148#, as dawsonite was detected in both sandstones and mudstones from these three wells.

The identified mudstones can be divided into caprocks and mudstone interlayers. The significance of caprocks in CO_2 gas reservoir is to prevent the escape of CO_2 to other reservoirs or to the surface. The 70-m-thick mudstones above SD10 in well H148# are cap mudstones, whereas the mudstones that occur between dawsonite-bearing sandstones in wells H145#, H146#, and H148# are mudstone interlayers. Thus, in these three wells, 10 dawsonite-bearing sandstone layers (SD 1 to SD 10) and 5 dawsonite-bearing mudstone layers (MD 1 to MD 5) can be identified in the Qingshankou Formation (Table. 2, Table 3). It is clear that dawsonite in the sandstones usually appears as multilayered zones of cementation which are separated by mudstone interlayers. The distance between each dawsonite-bearing sandstone layer ranges from 1.8 to 26.5 m. Dawsonite also presents in the mudstones no matter for the caprocks or mudstone interlayer. Besides dawsonite, ankerite was also found in some other mudstones; these mudstone layers are named as MA 1 to MA 3. Other mudstone layers, in which illite was well developed, are named as MI 1 and MI 2 (Fig. 7; Table 3).

Fluid inclusion characteristics

Four types of fluid inclusion (FI) are developed in dawsonite-bearing sandstones: aqueous inclusions (hydrocarbon-bearing saline inclusions), liquid (L-type) hydrocarbon-bearing inclusions, vapor (V-type) hydrocarbon-bearing inclusions, and liquid + vapor (L + V-type) hydrocarbon-bearing inclusions.

Aqueous inclusions (2 × 4 μm to 12 × 20 μm, vapor/liquid ratio < 5%) in gray, light gray, or light brown are distributed in quartz overgrowth and in cracks within dawsonite (Fig. 8b), calcite, and detrital quartz and have scattered or zoned distributions. The homogenization temperatures of these inclusions range from 71 to 127 °C with a mean of 93.5 °C, and the

Table 1 Contents for dawsonite cements and asphaltenes combining with well-logging data in dawsonite-bearing sandstones in Yaojia and Qingshankou Formations

Well	Depth (m)	Formation	Dawsonite (%)	Asphaltenes (%)	Well-logging data
H143	1256	K2y1	14	2.5	Oil layer
H143	1256.5	K2y1	9	0.9	Oil layer
H143	1257.86	K2y1	17	1.5	Oil layer
H143	1258.8	K2y1	16	1	Oil-water layer
H143	1553.65	K2qn2	15	3.8	Oil-water layer
H143	1598.7	K2qn2	13	7	Aqueous layer
H143	1599.15	K2qn2	13	4.1	Aqueous layer
H145	1476.5	K2qn2	8	1.5	/
H145	1491.1	K2qn2	8	4	/
H146	1506.66	K2qn2	12	4	Oil layer
H146	1506.9	K2qn2	14	1.5	Oil layer
H146	1507.21	K2qn2	13	0.7	Oil layer
H146	1508.16	K2qn2	19	7.2	Oil layer
H146	1518.35	K2qn2	16	5	Aqueous layer
H146	1518.65	K2qn2	12	0.9	Aqueous layer
H146	1519.7	K2qn2	12	1.3	Aqueous layer
H146	1545.95	K2qn1	12	3	/
H146	1548.46	K2qn1	6	2	/
H146	1548.9	K2qn1	13	2.4	/
H146	1550.11	K2qn1	9	4.2	/
H146	1550.21	K2qn1	18	6	/
H146	1550.41	K2qn1	16	3.3	/
H150	1548.91	K2qn1	13	2.8	Gas layer
H150	1556.38	K2qn1	12	3.2	Gas layer
H150	1556.8	K2qn1	10	2	Gas layer
H152	1536.05	K2qn2	10	4	Dry layer
H152	1536.15	K2qn2	11	3	Dry layer
H152	1536.45	K2qn2	14	1	Dry layer
H16	1587.27	K2qn1	2	1	Aqueous layer

salinity (wt.% NaCl equivalent) ranges from 1.74 to 14.41% with a mean of 5.70% (Table. 4). The aqueous inclusions typically coexist with L- and L + V-type hydrocarbon inclusions.

L-type hydrocarbon inclusions are gray or dark gray, with some displaying light-yellow or light-blue-green fluorescence. The L-type inclusions are abundant in intergranular quartz overgrowth and early-formed calcite, as well as along cracks in quartz overgrowth, in which they appear as discontinuous trails (Fig. 8a).

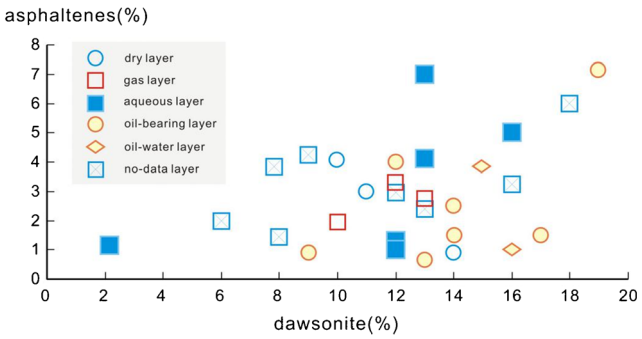

Fig. 6 Relationship between the dawsonite cements and asphaltenes in dawsonite-bearing sandstones

L + V-type hydrocarbon inclusions (2 × 6 μm to 15 × 20 μm, with vapor/liquid ratio < 5%) are distributed in the late-formed calcite and dawsonite (Fig. 8c, d) and along cracks in detrital quartz, detrital feldspar, and quartz overgrowth (Fig. 8e, f). The inclusions normally appear transparent or light yellow, and the contained liquid hydrocarbons show intense light-yellow and light-blue fluorescence. The homogenization temperatures of these inclusions range from 67 to 108 °C with a mean of 90.5 °C.

V-type hydrocarbon inclusions are gray and are found in clusters in late-formed calcite cements.

Two stages of inclusions can be distinguished based on their occurrences and the homogenization temperatures of coexisting aqueous inclusions (Fig. 9). The first stage comprises mainly L-type FIs and fewer L + V-type FIs, with some

Table 2 Framework and cement compositions of dawsonite-bearing sandstone in H145#, H146#, and H148# of Qingshankou Formation (according to Liu et al. 2011)

Well	Number	Depth (m)	Lithology	Samples	Q	F	L	**Daw**	Cc	Clay	Q_C
H145	SD1	1490.85 ~ 1491.5	Siltstone	4	33.25	19	26.25	**12**	6.25	0.75	2.5
	SD2	1486.5 ~ 1489	Siltstone	3	33	21	25	**6.8**	8.2	3	3
	SD3	1476 ~ 1477.3	Siltstone	2	34	18	27	**4.5**	11	3.5	1
	SD4	1464 ~ 1465.1	Siltstone	1	31	18	24	**12**	8	3	4
H146	SD5	1545.95–1550.41	Sandstone	7	32	18	25	**12**	10	1	3
	SD6	1518.1–1519.8	Sandstone	5	30.4	18.2	24.4	**13.4**	10.6	1	2
	SD7	1506.66–1508.16	Siltstone	4	30.7	15.5	25	**14.5**	12.5	0.8	1
H148	SD8	1483.12–1484	Sandstone	4	26.3	30.7	30.7	**5**	5		2.3
	SD9	1481.24–1482.25	Sandstone	7	25.5	28.8	25	**11**	2	5.2	2.5
	SD10	1477.97–1479.01	Sandstone	3	26	28	24	**11.8**	6.3	2	1.9

Q quartz, *F* feldspar, *L* lithic fragment, *Daw* dawsonite, *Cc* calcite cement, *Qc* quartz cement

of the inclusions displaying light-yellow fluorescence. These inclusions are distributed in the early-formed quartz overgrowth and early-formed calcite, or along cracks in early-formed quartz overgrowth, appearing as discontinuous trails. The inclusions that are developed in early-formed quartz overgrowth are mainly L-type hydrocarbon inclusions (GOI (grains with oil inclusions): 2–3%), with a few L + V hydrocarbon inclusions, whereas those that are developed in early-formed calcite are L hydrocarbon inclusions. The homogenization temperatures of the aqueous inclusions coexisting with the L inclusions are between 70 and 90 °C (Fig. 9).

The second stage of inclusions comprises mainly of L + V-type FIs (60–90% of the total), which are found surrounding quartz overgrowth and in detrital quartz as well as in calcite and dawsonite. Homogenization temperatures for aqueous inclusions coexisting with these inclusions are 100 to 120 °C (Fig. 9).

The oil charging recorded by these two stages of FIs identified in the dawsonite-bearing sandstones corresponds temporally to the periods of hydrocarbon charging: the first period is the accumulation of hydrocarbons occurring mainly at Neijiang-Mingshui period (Fig. 2), and the second stage is the late adjustment stage of the hydrocarbon reservoirs during formation uplifting. As the late-formed quartz and late-formed calcite, which contain the second-stage FIs, were formed after the dawsonite, it can be inferred that the CO_2 leading to the formation of the dawsonite occurred after the main period of petroleum accumulation.

Discussion

Formation of multilayer dawsonite-cemented zones

Thermodynamic analysis (Ryzhenko 2006) and geochemical numerical simulations (Xu and Pruess 2001; Xu et al. 2004; Pearce et al. 1996; Knauss et al. 2001, 2005; Neufeld et al. 2010; Gherardi et al. 2012; Kampman et al. 2014)

Table 3 X-ray diffraction data of mudstone interlayers and caprock in H145#, H146#, and H148# of Qingshankou Formation (according to Ming 2017)

Well	Number	Depth (m)	Lithology	Samples	Q	Kfs	Pl	Py	Hem	Daw	Ank	Sd	I/S	Ill
H145	MD1	1480–1480.02	Mudstone	1	47	6	15	–	5	**4**	–	–	6	17
	MD2	1435–1435.02	Mudstone	1	49	6	13	–	4	**2**	–	2	24 (Clay)	
H146	MA1	1541–1541.04	Mudstone	3	21.3	–	7.7	5.5	–	–	**13.1**	–	12.1	40.3
	MI1	1521 ~ 1523	Mudstone	7	24.8	2.2	15	2.4	0.8	–	2.6	3.2	9.5	39.5
	MI2	1516–1516.04	Mudstone	3	25.3	1.9	15.8	4.2	–	0	–	1.6	6.7	44.5
H148	MD3	1480.8–1480.84	Mudstone	4	15.6	3.5	13.9	3.6	–	**3.8**	5.4	3.2	25.8	25.2
	MD4	1477.5–1477.57	Mudstone	3	24.7	5.2	20.3	1.7	–	**2.3**	–	–	21.3	24.5
	MD5	1474.5–1474.6	Mudstone	1	20.6	–	15.8	1	–	**5.6**	–	–	57 (Clay)	
	MA2	1475.5 ~ 1476.56	Mudstone	8	23.1	1.6	12.9	3.7	–	–	**4.6**	5.7	21.6	26.8
	MA3	1473.5 ~ 1473.6	Mudstone	6	27.6	1.6	15.1	3.4	–	–	**4.6**	2	20.1	25.6

Q quartz, *Kfs* k-feldspar, *Pl* plagioclase, *Py* pyrite, *Hem* hematite, *Daw* dawsonite, *Ank* ankerite, *Sd* siderite, *I/S* illite and smectite mixing layer, *Ill* illite

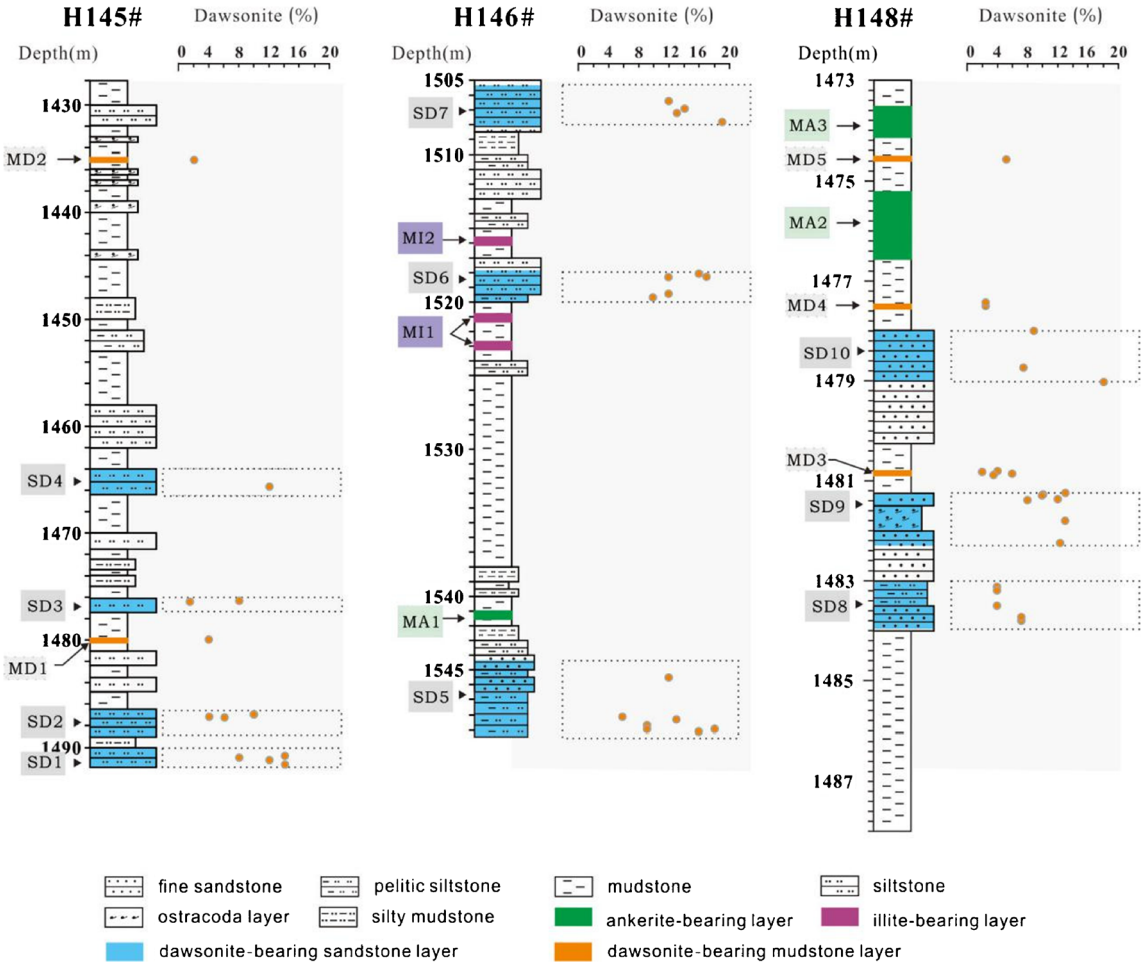

Fig. 7 Dawsonite appears as multilayered zones of cementation that are separated by mudstone interlayers. Ten dawsonite-bearing sandstone layers can be identified in the Qingshankou Formation in H145#, H146#, and H148#

indicated that CO_2, which was injected into the reservoir, would lead to the dissolution of the unstable minerals (feldspar, chlorite, carbonate minerals, etc.) and the precipitation of calcite, siderite, ankerite, or dawsonite. Combining with the paragenetic sequence, the minerals that formed after CO_2 flooding in Honggang are dawsonite, microcrystalline quartz II, kaolinite II, calcite II, and ankerite. The chemical reaction for the post-CO_2 injection of authigenic mineral formation in Honggang could be listed as Eqs. 1, 2, 3, 4, and 5.

$$\text{albite} + CO_2 + H_2O = \text{dawsonite} + 3\ \text{quartz} \quad (1)$$

(Knauss et al. 2005; Ryzhenko 2006)

$$\text{albite} + 2\ H^+ + 2\ Na^+ + 2\ CO_2\ (g) + 3\ H_2O = 2\ \text{dawsonite} + 2\ Ca^{2+} + 2\ \text{quartz} + \text{kaolinite} \quad (2)$$

(Ryzhenko 2006)

$$\text{albite} + 2\ H_2O + CO_2 = \text{calcite} + \text{kaolinite} \quad (3)$$

(Gunter et al. 1997; Suzanne and Spiers 2009)

$$\text{k feldspar} + Na^+ + 2CO_2(aq) + H_2O = \text{dawsonite} + 3\text{quartz} + 2K^+ \quad (4)$$

(Johnson et al. 2001; Cantucci et al. 2009)

$$\text{chlorite} + 5\ \text{calcite} + 5CO_2 = 5\ \text{ankerite} + \text{kaolinite} + \text{quartz} + 2H_2O \quad (5)$$

(Watson et al. 2004)

The formation of dawsonite requires elevated CO_2 partial pressure or abundant CO_3^{2-}/HCO_3^- anion, which means that the precipitation of dawsonite is usually found to be associated with massive CO_2 influx. The mineralogical assemblages (dawsonite and the other precipitated minerals) after CO_2 flooding are at thermodynamic equilibrium with a high pCO_2. As a function of the analysis on carbon-oxygen isotopic, it has been confirmed that the mantle-magmatic CO_2 provided the carbon sources for the deposited of dawsonite, calcite II, and ankerite (Liu et al. 2011).

Table 4 Homogenization temperature and salinity data of fluid inclusions in dawsonite-bearing sandstones

Well	Depth (m)	Host mineral	Inclusion type	Distribution type	Th (°C)	Salinity (wt.% Nacl)
H143	1599.15	Inner quartz overgrowth	L-type/aqueous	Zoned	71	6.16
H143	1599.15	Inner quartz overgrowth	Aqueous inclusion	Zoned	71	9.08
H143	1599.15	Inner quartz overgrowth	Aqueous inclusion	Zoned	72	5.86
H143	1599.15	Inner quartz overgrowth	L-type/aqueous	Zoned	73	7.31
H143	1553.65	Quartz	L-type/aqueous	Zoned	75	3.71
H143	1599.15	Inner quartz overgrowth	L-type/aqueous	Zoned	76	7.86
H143	1599.15	Inner quartz overgrowth	L-type/aqueous	Zoned	78	3.23
H143	1553.65	Quartz	L-type/aqueous	Zoned	79	4.03
H143	1599.15	Inner quartz overgrowth	Aqueous inclusion	Zoned	80	5.41
H143	1599.15	Inner quartz overgrowth	L-type/aqueous	Zoned	84	6.74
H143	1599.15	Dawsonite	Aqueous inclusion	Scattered	97	10.24
H143	1599.15	Quartz overgrowth	L-type/aqueous	Zoned	100	1.74
H143	1599.15	Quartz overgrowth	L-type/aqueous	Zoned	104	4.18
H143	1599.15	Quartz overgrowth	Aqueous inclusion	Scattered	104	5.11
H143	1599.15	Quartz overgrowth	Aqueous inclusion	Scattered	106	4.96
H143	1599.15	Quartz	Aqueous inclusion	Zoned	111	14.41
H143	1599.15	Quartz overgrowth	L-type/aqueous	Zoned	112	/
H143	1553.65	Quartz overgrowth	Aqueous inclusion	Scattered	117	/
H143	1553.65	Quartz overgrowth	aqueous inclusion	Scattered	122	/
H143	1553.65	Quartz	L + V-type/aqueous	Zoned	127	/
H146	1550.41	Quartz	L-type/aqueous	Zoned	74	6.74
H146	1550.41	Quartz	L-type/aqueous	Zoned	75	7.31
H146	1518.65	Quartz	L-type/aqueous	Zoned	76	4.8
H146	1518.65	Quartz	L-type/aqueous	Zoned	78	4.34
H146	1518.65	Quartz	L-type/aqueous	Zoned	80	3.55
H146	1550.41	Quartz	L-type/aqueous	Zoned	80	3.87
H146	1518.65	Quartz	L-type/aqueous	Zoned	82	/
H146	1550.41	Quartz	L-type/aqueous	Zoned	87	6.01
H146	1550.41	Quartz overgrowth	Aqueous inclusion	Scattered	94	5.26
H146	1518.65	Quartz	L + V-type/aqueous	Zoned	103	3.17
H146	1518.65	Quartz	L + V-type/aqueous	Zoned	106	1.74
H146	1518.65	Calcite	L + V-type/aqueous	Zoned	119	/
H146	1518.65	Quartz	L + V-type/aqueous	Zoned	119	/
H146	1550.41	Dawsonite	L + V-type/aqueous	Zoned	119	/
H146	1550.41	Quartz overgrowth	Aqueous inclusion	Scattered	120	/

Dawsonite presenting in mudstones could also be a product of a CO_2-water-rock system. Except for appearing as the product of the fracture filling, dawsonite, developing in mud sediments, was also reported in soil (Hay 1963), kaolinite mudstone (Limantseva et al. 2008), and oil shale (Smith and Milton 1966), and all of them had been considered to be related with the carbonate fluid induced by evaporation concentration. The stratum developing dawsonite in H145# and H148# is in fan delta front and shallow lake sedimentary system. In the stratigraphic sequence of southern Songliao Basin, there is no calcium crust which develops in the dawsonite-bearing soil as reported by Hay (1963) in Tanganyika (Oduvai) Gorge, or the characteristic minerals indicating evaporation environment (such as natural alkali and soda) developed in the dawsonite-bearing oil shale as Smith and Milton (1966) reported in the Green River Formation, Piceance Creek Basin of Colorado. Therefore, dawsonite developing in the mudstones of Honggang was probably the product induced by the upward diffusion of supercritical CO_2 through the underlying sandstones. CO_2 diffusion into clay-rich caprocks containing reactive phyllosilicate minerals and precipitation of carbonates was a suggested mechanism as previously predicted elsewhere (Haszeldine et al. 2005; Gherardi et al. 2012; Higgs et al. 2013, 2015; Watson et al. 2004; Xu et al. 2005).

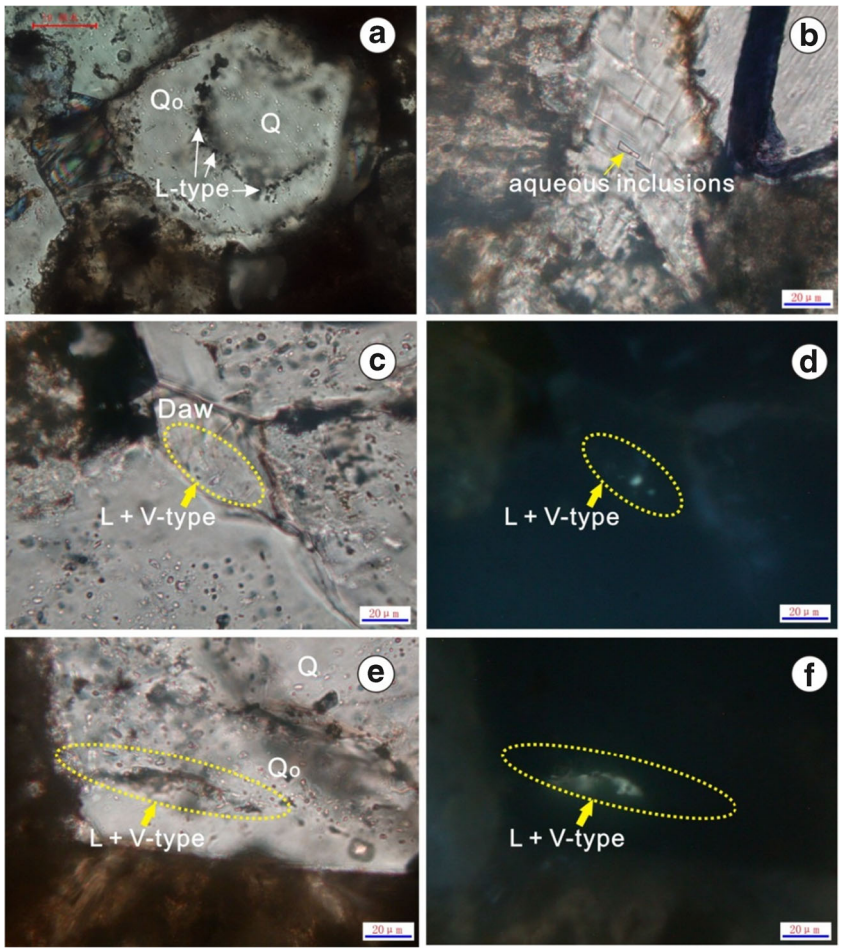

Fig. 8 Petrographic characteristics of fluid inclusions in dawsonite-bearing sandstones. (a) Dark gray L-type fluid inclusions in quartz overgrowth, H143#, 1599.15 m, plane polarized light; (b) aqueous fluid inclusion in dawsonite, H146#, 1518.65 m, plane polarized light; (c) L + V-type fluid inclusion in dawsonite, H146#, 1518.65 m, plane polarized light; (d) L + V-type fluid inclusion in dawsonite, the same site as (c), ultraviolet light; (e) L + V-type fluid inclusion in quartz overgrowth, H146#, 1550.41 m, plane polarized light; (f) L + V-type fluid inclusion in quartz overgrowth, the same site as (e), ultraviolet light. Q, quartz; Qo, quartz overgrowth; Daw, dawsonite; V-type liquid hydrocarbon-bearing inclusions; L + V-type liquid + vapor hydrocarbon-bearing inclusions

The injection of mantle CO_2 occurred in Paleogene, during that time the Qingshankou and Quantou Formation were with in situ pressures and temperatures in the range of 100–200 bar and 80–110 °C. With this pressure and temperature, CO_2 was in the supercritical state. The precipitation of a measurable quantity of minerals needs a significant quantity of water. If the reservoir is dry due to the presence of hydrocarbons (oil and gas) and/or water-free supercritical CO_2 ($scCO_2$), the precipitations of minerals are impossible and no record of the conditions is feasible, whereas, with the in situ pressures and temperatures, the dissolution of $scCO_2$ into bulk formation water generates carbonic acid, bicarbonate, and carbonate anions, leading to the bleaching of sandstones and formation of ferruginous carbonate concretions (Lewicki et al. 2007; Loope and Kettler 2015). In addition, the formation water will also be dissolved in $scCO_2$, forming a wet $scCO_2$ phase (Lin et al. 2008; Pearce et al. 2016), with the thickness of this phase measuring only a nanometer or angstrom on the surface of the mineral (Lin et al. 2008), leading mineral dissolution and precipitation induced by the wet $scCO_2$ phase limited.

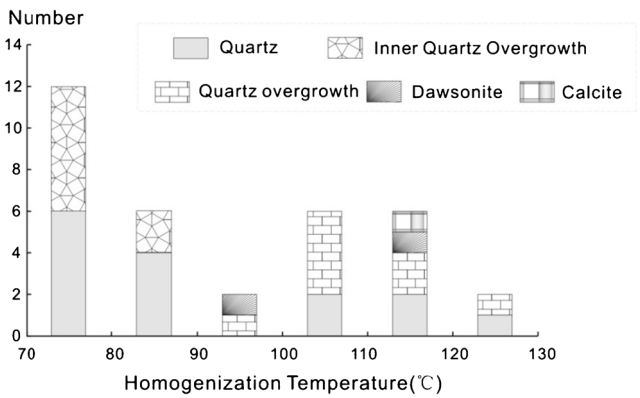

Fig. 9 Frequency histogram of the homogenization temperature in dawsonite-bearing sandstones

Normally the fractures could be the obvious migration "pathway" for $scCO_2$; moreover CO_2 can also migrate laterally along the connected sandstone layers or diffused upward through the low-permeability mudstone layers. During the upward diffusion, $scCO_2$ could migrate through the mudstone interlayer from the underlying sandstones and then transfer to the overlying sandstones. Ideally, the dissolved $scCO_2$ would have continued to diffuse into the overlying layers until it was exhausted. Simultaneously, dawsonite would have been precipitated in the sandstone and the mudstone interlayer, with

the content of dawsonite decreasing in the upper layers as the hypothesis shown in Fig. 10. In fact, the vertical distribution of the content of dawsonite in H145#, H146#, and H148# does not seem to change with the depth.

With the buffer of mudstones, $scCO_2$ tends to migrate laterally along the interworking sandstone layers. During the lateral migration, $scCO_2$ in the sandstones would have been distributed by the mudstone interlayer, following which multilayer dawsonite cementation would have occurred (Eqs. 1, 2, and 4) (Fig. 11).

Thereby, a multilayered dawsonite could be one of the geological produces for $scCO_2$ flooding through the heterogeneous rock, which acts as the lateral migration and upward diffusion.

According to the distribution of the dawsonite in caprocks and the mudstone interlayers, we can estimate the upper limit on the distance of diffusion of the dissolved $scCO_2$. Currently, we are not able to determine whether the formation of the ankerite and illite in the mudstones was related to the upward diffusion of $scCO_2$. The depth of MD5 is 1474.5 m, if dawsonite is assumed to be present in all of the mudstone interlayers from MD5 downward to the top of the underlying sandstone (1478 m), then the vertical distance of diffusion for this dissolved $scCO_2$ in the caprock mudstone is 3.5 m. If the whole mudstone interlayers (1480.5–1481.5 m) of MD3 contained dawsonite, then the distance of diffusion for this dissolved $scCO_2$ in the interlayered mudstone is only 1 m. Reactivity of the mudstone is generally shown to be low and limited to the vicinity of the CO_2-mudstone interface (Liu et al. 2012) and is related to the original mineralogical and petrophysical properties. The upward diffusion for $scCO_2$ to the low-permeability mudstone is limited. In the mudrock seals overlying a natural CO_2 reservoir in the North Sea Miller Oil Field, a total of 12 m vertically above the interface influenced by CO_2 was reported by Lu et al. (2009), which was evidenced by a strong linear upward decreasing trend of $\delta^{13}C$.

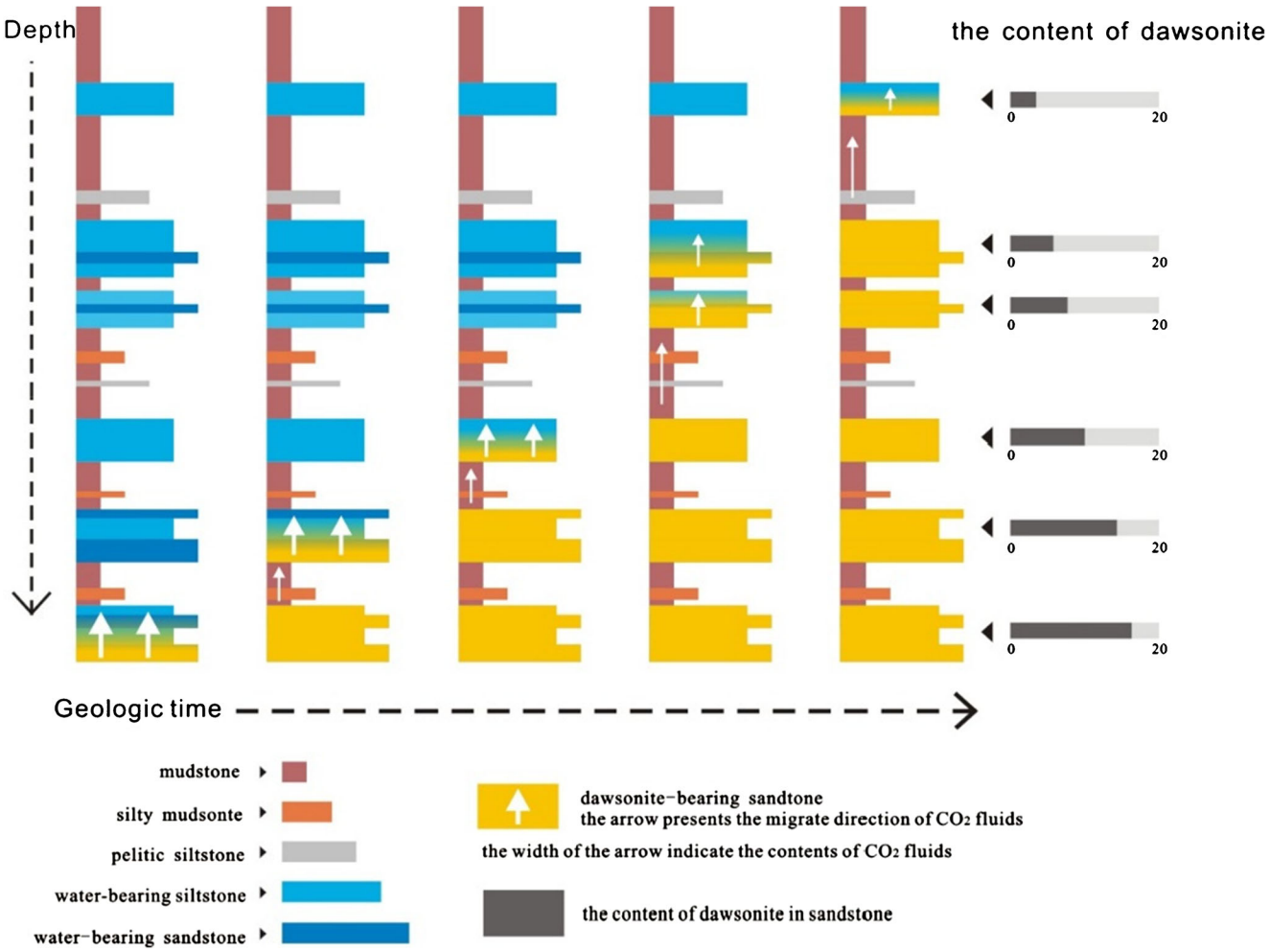

Fig. 10 Ideal pattern diagram for the upward diffusion of water-saturated supercritical CO_2 from underlying sandstone. Note the contents of dawsonite should be increased with depths

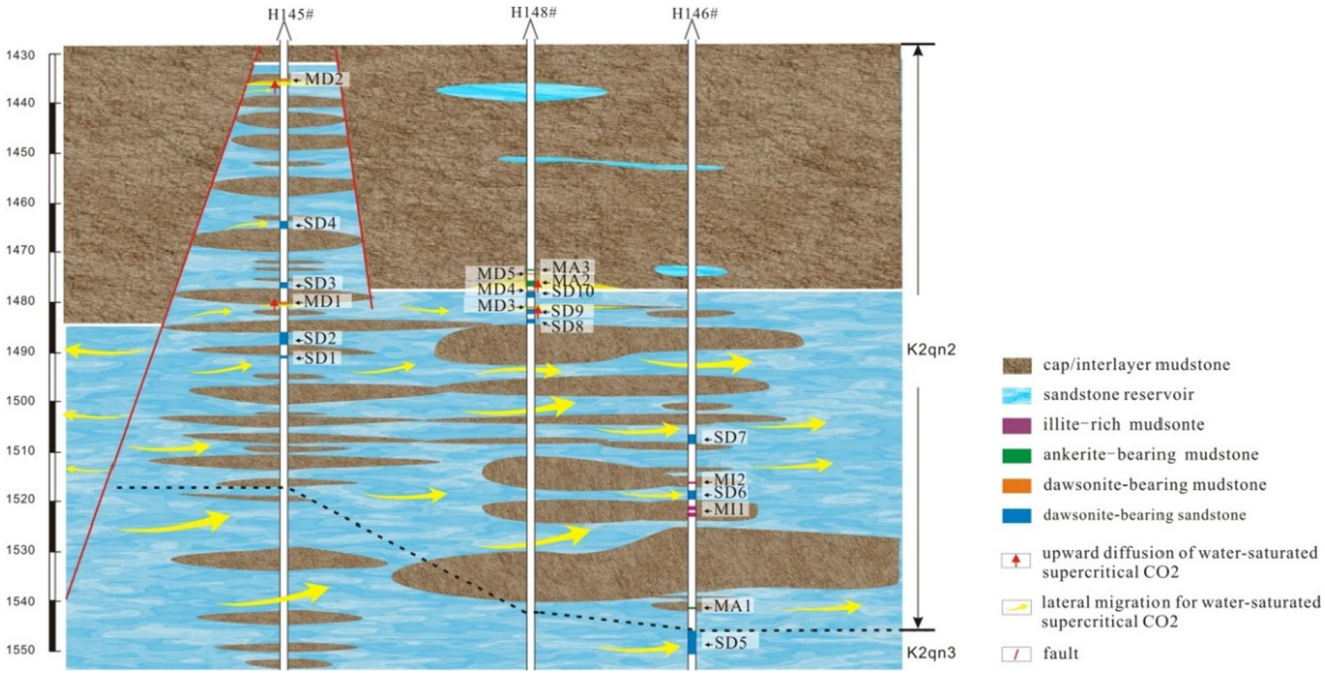

Fig. 11 Lateral migration and the upward diffusion of supercritical CO_2 from underlying sandstone lead to the formation of the multilayer dawsonite-cemented zones

Migration of CO_2 in dawsonite-bearing sandstones

As a function on the role of "CO_2 trace mineral" (Liu et al. 2009; Gao et al. 2009), the existence of dawsonite can record such a scenario, where a large-scale CO_2 is injected or resided in the geological history.

A typical CO_2-bearing reservoir is composed of upper water-free $scCO_2$ and lower dissolved $scCO_2$ into formation water. The geological record for water-free $scCO_2$ is rare, whereas dissolved $scCO_2$ can be recorded by the formation of carbonate minerals such as dawsonite and ankerite. Therefore, if dawsonite and $scCO_2$ coexisted in a CO_2-bearing reservoir, then the dawsonite cement layers can be regarded as the layers where the $scCO_2$ is dissolved in a sufficient quantity of water. If the reservoir is found to be with exhausted CO_2, then the dawsonite cement layers can be regarded as an ancient CO_2-bearing reservoir.

Dawsonite-bearing sandstone is normally well developed in CO_2-bearing reservoirs. For example, wells Su2# (1368–1450 m) and Wu10# (1811–1821 m) in the Hailar Basin (China) (Xu et al. 1994), Gu7# (1549.28–1577.14 m), Gu9# (1573.5–1579.5 m), Gu48# (1207.5–1515.7 m) in the Huazijing Step of the southern Songliao Basin (China) (Yu et al. 2014), and 22-1X State (462–472 m) in the Springerville–St. Johns CO_2 gas field (US) (Moore et al. 2005) all contain abundant dawsonite. However, CO_2 that is preserved in a dawsonite-bearing reservoir will eventually disappear by migrating to a new trap or leaking to the surface. CO_2 has been reported to have migrated to a new trap in wells Tong 1# and Wu 2# in the Hailar Basin (China) (Xu et al. 1994) and undergone small-scale leakage in the Shabwa Basin (Yemen) (Worden 2006), Fuxin Basin (China) (Liu et al. 2008), and Tamtsag Basin (Mongolia) (Liu et al. 2009).

Dawsonite-bearing sandstones are widespread in 14 wells, but most wells in the anticline do not contain CO_2. CO_2 is distributed in several wells which are mostly on the northeastern part of the anticline, such as H73# and H77# (Zou et al. 2007), with dawsonite-bearing sandstones and CO_2 gas coexisting only in well H73#. The C isotope values ($\delta^{13}C$, PDB) of dawsonite in the sandstones of the Honggang anticline range from −3.42 to 3.29‰, whereas the C isotope values of CO_2 in isotopic equilibrium with dawsonite ($\delta^{13}C_{CO2}$, PDB) are calculated to be in the range of −9.92 to −4.23‰ (Liu et al. 2011). This is calculated using the calcite-CO_2 carbon isotope fractionation equation of Ohmoto and Rye (1979), and assuming there is zero carbon isotope fractionation between calcite and dawsonite, the temperature for this equation was calculated by the depth of dawsonite-bearing sandstones (1256 ~ 1830 m) and the average geothermal gradient (4.26 °C/100 m). The calculated $\delta^{13}C_{CO2}$ values are similar to the carbon isotope values ($\delta^{13}C$, PDB) of the residual CO_2 in the gas reservoir (−8.05 to −2.65‰) (Hou et al. 2009), suggesting that CO_2 for dawsonite genesis and residual CO_2 in the gas reservoir of the Honggang anticline had the same carbon source. Dawsonite could provide a permanent mineral storage host only in systems that maintain high CO_2 pressures; once high CO_2 pressure dissipates, dawsonite may be an ephemeral phase in dynamic setting (Hellevang et al. 2005). This means that in addition to the CO_2 trapped by the precipitation of dawsonite, the remaining

free or dissolved CO_2 would still be existing in the reservoir. Combined with the truth that most of the present CO_2 gas reservoirs (in K1q4) are in the deeper layers than the dawsonite-bearing sandstone reservoirs without CO_2 (K1q4-K2y1), we can deduce that CO_2 was at some time abundant in the Honggang anticline (in K1q4-K2y1) but had now part of CO_2 been migrated to the north part of the anticline or to other traps, with the other part consumed by the reaction with the primary rock, producing new carbonates. With the basic thermodynamic fraction equation and geological numerical simulations, CO_2 sequestered by dawsonite-bearing sandstones was calculated to be 89.73 ~ 99.51 kg/m^3 (Liu et al. 2011).

Hydrocarbon filling events were also recorded in the dawsonite-bearing sandstones by the paragenesis and compositions of fluid inclusions. In Honggang, parts of the dawsonite-bearing sandstones are developed in oil-bearing or oil-water layers. Two stages of hydrocarbon-bearing (oil-gas) inclusions were found in the dawsonite-bearing sandstones, with the later-stage inclusions (presenting the adjustment stage of the hydrocarbon) being contained in the microcrystalline quartz II, calcite II, and dawsonite, as well as in fractures in the quartz grains, quartz overgrowth, and detrital feldspar (Fig. 8). The diagenetic sequence indicates that dawsonite, microcrystalline quartz II, and calcite II were formed after CO_2 flooding. Therefore, we infer that the injection time of CO_2 and the adjustment stage of the hydrocarbon were separated by only a very short time interval. The second-stage FIs, most of which were L + V-type hydrocarbon-bearing inclusions and distributed in fractures/cracks in quartz grains and their overgrowth, were found to contain not only CO_2 in both gaseous and liquid phases but also CO_3^{2-} with CH_4 (Qu et al. 2013). Inorganic CO_2 was detected in the northeastern part of the anticline (well H73#), with $\delta^{13}C_{PDB}$ values between − 5.32 and − 5.80‰ (Hou et al. 2009), indicating that inorganic CO_2 has dissolved in the oil. The physical and chemical properties of crude oil and the ionic concentration of formation water were also changed after the CO_2 injection (Yu et al., 2016). The change of crude oil shows the decrease of density, viscosity, freezing point, and initial boiling point, while the change of formation water is the increase of salinity, K^++Na^+, and HCO_3^-.

Asphaltenes, abundant in the dawsonite-bearing sandstones, might be a product induced by deasphalting of crude oil through injection of mantle-derived CO_2. The principal processes for the asphaltene formation generated with crude oil include thermal alteration and deasphalting (Rogers et al. 1974; Leythaeuser and Anf Rückheim 1989; Larter et al. 1990; Wilhelms and Larter 1994, 1995; Hunt 1996; Huc et al. 2000; Liu et al. 2020b). The process for the direct thermal cracking of petroleum hydrocarbons usually occurs at great depths (temperatures of ≥ 170 °C; Milner et al. 1977; Huc et al. 2000; Waples 2000). However, the maximum burial temperature from the burial-thermal history models (~ 117 °C) or the higher temperature recorded in fluid inclusions (122 °C) does not exceed the lowermost temperature boundary for thermal alteration (170 °C). This indicated that very little thermal alteration of crude oil occurred in the Qingshankou Formation reservoir.

It is well known that the flooding of CO_2 into an oil reservoir could cause the precipitation of asphaltenes (Novosad and Costain 1990; Monger and Trujillo 1991; Liu et al. 2020a). As the solubility of CO_2 in oil is nearly 30 times higher than that in pure water, CO_2 dissolved in oil reduces the viscosity of the oil and increases its volume, thereby providing the internal driving energy for this oil. Characterizing such mechanisms will assist in enhanced oil recovery (CO_2-EOR), which has been applied to projects in various countries (Blunt et al. 1993; Kovscek and Cakici 2005; Han and McPherson 2009; Lindeberg et al. 2017; Lee et al. 2019). When CO_2 dissolves in oil, the dynamic equilibrium of the original chemical composition of the oil is altered, followed by fractionation of light components and enrichment of heavy components, causing the precipitation of asphaltenes.

In Honggang, asphaltenes develop in the intergranular pores of residual dawsonite aggregations, and there is a moderate positive relationship between the contents of asphaltenes and dawsonite cements. We can deduce that the crude oil in this area was deasphalted after the injection of CO_2, with the residual lighter oil trapped as hydrocarbon fluid inclusions in carbonate minerals such as dawsonite. This is in turn suggested that CO_2 could be stored as carbonate minerals after the termination of a CO_2-EOR project.

Conclusions

We examined the occurrence of dawsonite cements as well as the characteristics of fluid inclusions in dawsonite-bearing sandstones of the Honggang anticline, southern Songliao Basin, to establish a petrological record of magmatic CO_2 migration in the heterogeneity reservoir. Our conclusions are as follows:

1. Dawsonite normally appears as multilayered zones of cementation in the sandstones which are separated by mudstone interlayers. These multilayered dawsonite could be one of the geological produces for mantle-derived CO_2 flooding through the heterogeneous rock, which acts as the lateral migration and upward diffusion.
2. Dawsonite was detected in the mudstone interlayers, which implied CO_2 could migrate through the thinner mudstone interlayer from the underlying sandstones and then transfer to the overlying sandstones. The vertical distance of diffusion for this dissolved scCO_2 in the mudstones is limited. Caprock is still efficient to prevent the escape of CO_2 to other reservoirs or to the surface.

3. Both of the hydrocarbon and mantle CO_2 injection events have been recorded in the dawsonite-bearing sandstones. Combined with the truth that the injection time of CO_2 is later than that of hydrocarbon, the deasphalting of crude oil by injection of mantle-derived CO_2 should occur, with the asphaltenes as the deasphalting product, abundant in dawsonite-bearing sandstones. Therefore, CO_2 could also be stored as long-term carbonate minerals, such as dawsonite, after the termination of a CO_2-EOR project.

Acknowledgments Thanks are given to the teams at the Analytical Laboratory Beijing Research Institute of Uranium Geology for performing fluid inclusion analysis. This research was supported by the National Natural Science Foundation of China (No. 41202073, No.41572082) and National Major Scientific and Technological Special Project during the Twelfth Five-year Plan Period (No. 2011ZX05025-002).

References

Al-Khdheeawi EA, Vialle S, Barifcani A, Sarmadivaleh M, Iglauer S (2018) Effect of wettability heterogeneity and reservoir temperature on CO_2 storage efficiency in deep saline aquifers. Int J Greenhouse Gas Control 68:216–229

Álvarez-Ayuso E, Nugteren HW (2005) Synthesis of dawsonite: a method to treat the etching waste streams of the aluminium anodising industry. Water Res 39(10):2096–2104

Aminu MD, AliNabavi S, Rochelle CA, Manovic V (2017) A review of developments in carbon dioxide storage. Appl Energy 208:1389–1419

Baker JC, Bai GP, Hamilton PJ, Golding SD, Keene JB (1995) Continental-scale magmatic carbon dioxide seepage recorded by dawsonite in the Bowen-Gunnedah-Sydney basin system, eastern Australia. J Sediment Res 65:522–530

Bénézeth P, Palmer DA, Anovitz LM, Horita J (2007) Dawsonite synthesis and reevaluation of its thermodynamic properties from solubility measurements. Geochim Cosmochim Acta 71:4438–4455

Blunt M, Fayers FJ, Orr FM Jr (1993) Carbon dioxide in enhanced oil recovery. Energy Convers Manag 34:1197–1204. https://doi.org/10.1016/0196-8904(93)90069-M

Cantucci B, Montegrossi G, Vaselli O, Tassi F, Quattrocchi F, Perkins EH (2009) Geochemical modeling of CO storage in deep reservoirs: the Weyburn project (Canada) case study. Chem Geol 265(1–2):181–197

Chen FJ, Zhao HL, Chen ZN (1996) Structural characteristics and geodynamic setting of Mesozoic and Cenozoic extensional basins in eastern China. Earth Sci 21(4):357–365 [in Chinese with English abstract]

Chen GL (2003) Revaluation and supplementary exploration of several new formations of Honggang structure. Petroleum Geology & Oilfield Development in Daqing 22(1):10–12 [in Chinese with English abstract]

Dai JX, Song Y, Dai CS, Chen AF, Sun ML, Liao YS (1995) Inorganic origin gas and formation condition of the kind of gas reservoir. Science Press, Beijing [in Chinese]

Fu XF, Sha W, Wang L, Liu XB (2010) Distribution law of mantle–origin CO gas reservoirs and its controlling factors in Songliao Basin. Journal of Jilin University (Earth Science Edition) 40:253–262 [in Chinese with English abstract]

Gao JY, Shi BQ, Wang L, Dou LR, Cheng DS, Pan XH (2009) A typical case of heavy oil pool with the origin of CO_2 deasphaltizing. Geoscience 23(5):923–927 [In Chinese with English abstract]

Ge RF, Zhang QL, Wang LS, Chen J, Xie GA, Wang XY (2012) Late Mesozoic rift evolution and crustal extension in the central Songliao Basin, northeastern China: Constraints from cross-section restoration and implications for lithospheric thinning. Int Geol Rev 54:183–207. https://doi.org/10.1080/00206814.2010.511900

Gherardi F, Audigane P, Gaucher EC (2012) Predicting long-term geochemical alteration of wellbore cement in a generic geological CO_2 confinement site. J Hydrol 420–421:340–359

Giuliano A, Catizzone E, Barisano D, Nanna F, Villone A, De Bari I, Cornacchia G, Braccio G (2019) Towards methanol economy: a techno-environmental assessment for a bio-methanol OFMSW/biomass/carbon capture-based integrated plant. Int J Heat Technol 37(3):665–674. https://doi.org/10.18280/ijht.370301

Golab AN, Carr PF, Palamara DR (2006) Influence of localised igneous activity on cleat dawsonite formation in late Permian coal measures, upper Hunter Valley, Australia. Int J Coal Geol 66(4):296–304

Gunter WD, Wiwchar B, Perkins EH (1997) Aquifer disposal of CO -rich greenhouse gases: extension of the time scale of experiment for CO -sequestering reactions by geochemical modelling. Mineral Petrol 59:121–140

Han WS, McPherson BJ (2009) Optimizing geologic CO_2 sequestration by injection in deep saline formations below oil reservoirs. Energy Convers Manag 50:2570–2582. https://doi.org/10.1016/j.enconman.2009.06.008

Haszeldine RS, Quinn O, England G, Wilkingson M, Shipton ZK, Evans JP, Heath J, Crossey L, Ballentine CJ, Graham CM (2005) Natural geochemical analogues for carbon dioxides to rage in deep geological porous reservoirs, a UK perspective. In Special Issue Oil Gas Sci Technol 60:33–49

Hay RL (1963) Zeolitic weathering in Olduvai Gorge, Tanganyika. Geol Soc Am Bull 74(10):1281

Hellevang H, Aagaard P, Oelkers EH, Kvamme B (2005) Can dawsonite permanently trap CO_2? Environ Sci Technol 39:8281–8287

Hellevang H, Aagaard P, Jahren J (2014) Will dawsonite form during CO_2 storage? Greenhouse Gas Sci Technol 4:191–199

Higgs KE, Funnell RH, Reyes AG (2013) Changes in reservoir heterogeneity and quality as a response to high partial pressures of CO2 in a gas reservoir, New Zealand. Mar Pet Geol 48:293–322

Higgs KE, Haese RR, Golding SD, Schacht U, Watson MN (2015) The Pretty Hill formation as a natural analogue for CO storage: an investigation of mineralogical and isotopic changes associated with sandstones exposed to low, intermediate and high CO concentrations over geological time. Chem Geol 399:36–64

Hou QJ, Zhao ZK, Wang LW (2009) Heterogeneity of oil composition within a reservoir as a reflection of accumulation history. In: Volcanic gas reservoir principle & exploration: example from southern Songliao Basin. Science Press. In Chinese with English abstract, Beijing. https://doi.org/10.1016/0016-7037(89)90330-X

Huc AY, Nederlof P, Debarre R, Carpentier B, Boussafir M, Laggoun-Défarge F, Lenail-Chouteau A, Bordas- Le Floch N (2000) Pyrobitumen occurrence and formation in a Cambro-Ordovician sandstone reservoir, Fahud salt Basin, north Oman. Chem Geol 168:99–112. https://doi.org/10.1016/S0009-2541(00)00190-X

Hunt JM (1996) Petroleum geochemistry and geology. W.H. Freeman, San Francisco

IPCC (2005) Special report on carbon dioxide capture and storage. Cambridge University Press, UK

Johnson JW, Nitao JJ, Steefel CI (2001) Reactive transport modeling of geologic CO sequestration in saline aquifers: the influence of intra-aquifer shales and the relative effectiveness of structural, solubility, and mineral trapping during prograde and retrograde sequestration. In: Washington D C. National Energy Technology Laboratory, US Department of Energy

Kampman N, Bickle M, Wigley M, Dubacq B (2014) Fluid flow and CO2-fluid-mineral interactions during CO2-storage in sedimentary basins. Chem Geol 369:22–50

Karimi KG, Ebrahimi M, Mozaffari SA (2018) ZnO-carbon active nanostructured thin film fabrication by spin coating technique for enzymatic urea biosensing. J New Mater Electrochem Syst 21(2):81–89

Kaszuba JP, Viswanathan HS, Carey JW (2011) Relative stability and significance of dawsonite and aluminum minerals in geologic carbon sequestration. Geophys Res Lett 38 L08404. https://doi.org/10.1029/2011GL046845

Knauss KG, Johnson JW, Steefel CI, Nitao JJ (2001) Evaluation of the impact of CO, aqueous fluid, and reservoir rock interactions on the geologic sequestration of CO, with special emphasis on economic implications, in first National Conference on carbon sequestration. National Energy Technology Laboratory, Washington, D.C., pp 26–37

Knauss KG, Johnson JW, Steefel CI (2005) Evaluation of the impact of CO_2, CO-contaminant gas, aqueous fluid and reservoir rock interactions on the geologic sequestration of CO_2. Chem Geol 217:339–350

Kovscek AR, Cakici MD (2005) Geologic storage of carbon dioxide and enhanced oil recovery. II. Cooptimization of storage and recovery. Energy Convers Manag 46:1941–1956. https://doi.org/10.1016/j.enconman.2004.09.009

Larter SR, Bjørlykke KO, Karlsen DA, Nedkvitne T, Eglinton TI, Johansen PE, Leythaeuser D, Mason PC, Mitchell AW, Newcombe GA (1990) Determination of petroleum accumulation histories examples from the Ula field, Central Graben, Norwegian North Sea: North Sea oil and gas reservoirs II. Graham and Trotman, London, pp 319–330

Lee E, Hornafius JS, Dean E, Kazemi H (2019) Potential of Denver basin oil fields to store CO_2 and produce bio-CO_2-Eor oil. Int J Greenhouse Gas Control 81:137–156

Lewicki JL, Birkholzer JT, Tsang CF (2007) Natural and industrial analogues for leakage of CO_2 from storage reservoirs: identification of features, events, and processes and lessons learned. Environ Geol 52(3):457–467

Leythaeuser D, Anf Rückheim J (1989) Heterogeneity of oil composition within a reservoir as a reflection of accumulation history. Geochim Cosmochim Acta 53:2119–2123

Limantseva OA, Makhnach AA, Ryzhenko BN, Cherkasova EV (2008) Formation of dawsonite mineralization at the Zaozernyi deposit, Belarus. Geochem Int 46(1):62–76

Lin HF, Fujii T, Takisawa R, Takahashi T, Hashida T (2008) Experimental evaluation of interactions in supercritical CO_2/water/rock minerals system under geologic CO_2 sequestration conditions. J Mater Sci 43(7):2307–2315

Lindeberg E, Grimstad A, Bergmo P, Wessel-Berg D, Torsaeter M, Holt T (2017) Large scale tertiary CO2 EOR in mature water flooded Norwegian oil field. Energy Procedia 114:7096–7106

Liu YZ, Luo H, Liu X (2008) Characterization of shallow tight sandstone reservoir and diagenesis of K1sh3 in the Fuxin basin. Contribut Geol Min Resourc Res 23(1):77–81

Liu L, Zhu DF, Qu XY, Jin ZL, Wang XQ, Dong LS (2009) Impacts of mantle-genetic CO_2 influx on the reservoir quality of Lower Cretaceous sandstone from Wuerxun depression, Hailar basin. Acta Petrol Sin 25(10):2311–2319

Liu N, Liu L, Qu XY, Yang HD, Wang LJ, Zhao S (2011) Genesis of authigene carbonate minerals in the Upper Cretaceous reservoir, Honggang anticline, Songliao Basin: a natural analogue for mineral trapping of natural CO_2 storage. Sediment Geol 237:166–178. https://doi.org/10.1016/j.sedgeo.2011.02.012

Liu FY, Lu P, Griffith C, Hedges WS, Soong Y, Hellevang H, Zhu C (2012) CO_2–brine–caprock interaction: reactivity experiments on Eau Claire shale and a review of relevant literature. Int J Greenhouse Gas Control 7:153–167

Liu XB, Fu XF, Liu DM, Wei W, Lu XS, Liu CB, Wang WA, Gao HJ (2018) Distribution of mantle-derived CO_2 gas reservoir and its relationship with basement faults in Songliao Basin, China. J Natural Gas Sci Eng 56:593–607

Liu B, Yang Y, Li J, Chi Y, Li J, Fu X (2020a) Stress sensitivity of tight reservoirs and its effect on oil saturation: a case study of Lower Cretaceous tight clastic reservoirs in the Hailar Basin, Northeast China. J Pet Sci Eng 184:106484. https://doi.org/10.1016/j.petrol.2019.106484

Liu B, Song Y, Zhu K, Su P, Ye X, Zhao W (2020b) Mineralogy and element geochemistry of salinized lacustrine organic-rich shale in the middle Permian Santanghu Basin: implications for paleoenvironment, provenance, tectonic setting and shale oil potential. Mar Pet Geol 120:104569

Loope DB, Kettler RM (2015) The footprints of ancient CO_2 -driven flow systems: ferrous carbonate concretions below bleached sandstone. Geosphere 11(3):943–957

Lu J, Wilkinson M, Haszeldine RS, Fallick AE (2009) Long-term performance of a mudrock seal in natural CO_2 storage. Geology 37:35–38

Milner CWD, Rogers MA, Evans CR (1977) Petroleum transformations in reservoirs. J Geochem Explor 7:101–153. https://doi.org/10.1016/0375-6742(77)90079-6

Ming XR (2017) Geologic records of CO_2-bearing fluids–argillaceous rocks interaction and their effects on sealing ability of cap rocks. Jilin University, Changchun [In Chinese with English abstract]

Monger TG, Trujillo DE (1991) Organic deposition during CO_2 and rich-gas flooding. SPE Reserv Eng 6:17–24

Moore J, Adams M, Allis R, Lutz S, Rauzi S (2005) Mineralogical and geochemical consequences of the long-term presence of CO_2 in natural reservoirs: an example from the Springerville–St. Johns Field, Arizona, and New Mexico, USA. Chem Geol 217:365–385. https://doi.org/10.1016/j.chemgeo.2004.12.019

Neufeld JA, Hesse MA, Riaz A, Hallworth MA, Tchelepi HA, Huppert HE (2010) Convective dissolution of carbon dioxide in saline aquifers. Geophys Res Lett 37(12):L22404. https://doi.org/10.1029/2010GL044728

Niu SZ, Hu WS, Xiong P, Li XM, Huang YX (2012) Lithofacies study of Gaotaizi reservoir in Honggang oilfield. J Oil and Gas Technol 34(6):43–47

Noh H, Kang K, Huh C, Kang S, Seo Y (2018) Identification of potential hazardous events of unloading system and CO2 storage tanks of an intermediate storage terminal for the Korea clean carbon storage project 2025. Int J Saf Sec Eng 8(2):258–265. https://doi.org/10.2495/SAFE-V8-N2-258-265

Novosad Z and Costain TG (1990) Experimental and modeling studies of asphaltene equilibria for a reservoir under CO2 injection. In SPE Annual Technical Conference and Exhibition. Society of Petroleum Engineers

Okuyama Y, Sasaki M, Nakanishi S, Todaka N, Ajima S (2009) Geochemical CO_2 trapping in open aquifer storage- the Tokyo Bay model. Energy Procedia 1:3253–3258. https://doi.org/10.1016/j.egypro.2009.02.110

Park H, Jiang LL, Kiyami T, Zhang Y, Ueda R, Nakano M, Xue ZQ (2017) Influence of sedimentation heterogeneity on CO_2 flooding. Energy Procedia 114:2933–2941

Pearce JM, Holloway S, Wacker H, Nelis MK, Rochelle C, Bateman K (1996) Natural occurrences as analogues for the geological disposal of carbon dioxide. Energy Convers Manag 37:1123–1128. https://doi.org/10.1016/0196-8904(95)00309-6

Pearce JK, Dawson GKW, Law ACK, Biddle D, Golding SD (2016) Reactivity of micas and cap-rock in wet supercritical CO_2 with SO_2 and O_2 at CO_2 storage conditions. Appl Geochem 72:59–76

Ren ZL, Xiao DM, Chi YL (2001) Restoration of the palaeogeotherm in Songliao basin. Petroleum Geology & Oilfield Development in Daqing 20(1):13–14,55 [in Chinese with English abstract]

Ryzhenko BN (2006) Genesis of dawsonite mineralization: thermodynamic analysis and alternatives. Geochem Int 44(8):835–840

Qiao YJ, Zhu GW, Li XF, Bai B, Li J, Wang YS, Zhao XL, Zhang B (2020) Characterizing CO_2 plume migration in multi-layer reservoirs with strong heterogeneity and low permeability using time-lapse 2D VSP technology and numerical simulation. Int J Greenhouse Gas Control 92:1–12

Qu XY, Yang HD, Liu L, Liu N, Qi Z, Tang H (2013) The genesis and its impaction on oil and gas reservoir of oil-associated CO2 in southern part of Songliao Basin. J Jilin Univ (Earth Sci Ed) 43:39–48

Qu XY, Chen X, Yu M, Liu L (2016) Mineral dating of mantle-derived CO_2 charging and its application in the southern Songliao Basin, China. Appl Geochem 68:19–28

Rogers MA, McAlary JD, Bailey NJL (1974) significance of reservoir bitumens to thermal-maturation studies, Western Canada Basin. Am Assoc Pet Geol Bull 5(58):1806–1824

Shi Y, Huang XC, Feng GH (2019) Wellbore-reservoir coupling simulation of geochemical reactions involving carbon dioxide. Int J Heat Technol 37(3):811–819. https://doi.org/10.18280/ijht.370318

Shin JW, Son JT (2018) Improvement of electrochemical performance and thermal stability by reducing residual lithium hydroxide on LiNi0.8Co0.1Mn0.1O2 active material using amorphous carbon coating. J New Mater Electrochem Syst 21(2):71–75

Smith JW, Milton C (1966) Dawsonite in the Green River formation of Colorado. EconomicGeology 61:1029–1042

Suzanne JT, Spiers CJ (2009) Reaction of plagioclase feldspars with CO under hydrothermal conditions. Chem Geol 265(1–2):88–98

Wang LJ (2013) Characteristics and mechanisms of interactions between CO_2 fluids and mudstones: an example from southern Songliao Basin. Jilin University, Changchun

Waples DW (2000) The kinetics of in-reservoir oil destruction and gas formation: constraints from experimental and empirical data, and from thermodynamics. Org Geochem 31:553–575. https://doi.org/10.1016/S0146-6380(00)00023-1

Watson MN, Zwingmann N, Lemon NM (2004) The Ladbroke grove–Katnook carbon dioxide natural laboratory: a recent CO accumulation in a lithic sandstone reservoir. Energy 29(9–10):1457–1466

Wilhelms A, Larter SR (1994) Origin of tar mats in petroleum reservoirs. Part II: Formation mechanisms for tar mats. Mar Pet Geol 11:442–456. https://doi.org/10.1016/0264-8172(94)90078-7

Wilhelms A, Larter SR (1995) Overview of the geochemistry of some tar mats from the North Sea and USA: implications for tar-mat origin, The geochemistry of reservoirs: Geological Society, London, Special Publications, 86, 87–101. https://doi.org/10.1144/GSL.SP.1995.086.01.07

Worden RH (2006) Dawsonite cement in the Triassic Lam Formation, Shabwa basin, Yemen: a natural analogue for a potential mineral product of subsurface CO_2 storage for greenhouse gas reduction. Mar Pet Geol 23:61–77

Wu YD, Zhao WZ, Zou CN, Li M, Wu XS (2006) Study on hydrocarbon accumulation of litho-stratigraphic traps in southern Songliao Basin. Xinjiang Pertroleum Geol 27:19–22

Xu YB, Chen P, Xu YC (1994) Dawsonite distribution and its relationship with oil and gas in Halar basin. Oil Gas Geol 15(4):322–327

Xu M, Middleton MF, Xue LF, Wang DP (2000) Structure of the lithosphere and Mesozoic sedimentary basins in western Liaoning, northern Liaoning, and Songliao, Northeast China. Int Geol Rev 42:269–278. https://doi.org/10.1080/00206810009465082

Xu T, Pruess K (2001) Modeling multiphase non-isothermal fluid flow and reactive geochemical transport in variably saturated fractured rocks: 1. Methodology American Journal of Science 301(1):16–33

Xu T, Apps JA, Pruess K (2004) Numerical simulation of CO disposal by mineral trapping in deep aquifers. Appl Geochem 19(6):917–936

Xu T, Apps JA, Pruess K (2005) Mineral sequestration of carbon dioxide in a sandstone–shale system. Chem Geol 217(3–4):295–318

Yang G, Zhao ZY, Wang W (2010) Distribution and accumulation of inorganic CO_2 in southern Songliao Basin. J Jilin Univ (Earth Sci Ed) 40(4):932–938

Yu M, Liu L, Yu ZC, Liu N, Yang HD, Qu XY (2014) Dawsonite fixation of mantle CO_2 in the cretaceous Songliao Basin, Northeast China: a natural analogue for CO_2 mineral trapping in oilfields. Int Geol Rev 56(14):1792–1812. https://doi.org/10.1080/00206814.2014.958765

Zhang HH (2006) Geochemistry of late Mesozoic-Cenozoic basalts from Yitong-Datun and Shuangliao area, Northeast China: Implication for lithospheric evolution and the involvement of the recycled Pacific Oceanic crust in basalt genesis. Chinese Academy of Sciences, Beijing

Zhang XF, Wen ZY, Gu ZH, Xu XH, Lin ZX (2004) Hydrothermal synthesis and thermodynamic analysis of dawsonite-type compounds. J Solid State Chem 177(3):849–855

Zhang Z, Bao ZD (2009) Development characteristics and controlling factors of reservoir fractures in Chaoyanggou oilfield, Songliao Basin. Earth Sci Front 16:166–172

Zhao S, Liu L, Liu N (2018) Petrographic and stable isotopic evidences of CO2-induced alterations in sandstones in the Lishui sag, East China Sea Basin, China. Appl Geochem 90:115–128. https://doi.org/10.1016/j.apgeochem.2018.01.004

Zou CN, Jia CZ, Zhao WZ, Tao SZ, Gu ZD, Hou QJ, Zhao ZY, Song LZ (2005) Accumulation dynamics and distribution of lithostratigraphic reservoirs in south Songliao Basin. Pet Explor Dev 32:324–130

Zou CN, Tao SZ, Zhang YY (2007) Reservoir-forming age and its exploration significance to stratigraphic reservoirs in southern Songliao Basin. Chin Sci Bull 52:3239–3252. https://doi.org/10.1007/s11434-007-0424-5